Chapter 7
Dynamic Simulation of Mechanical Fluid Separation in Solid Bowl Centrifuges

Marco Gleiss and Hermann Nirschl

Abstract Solid bowl centrifuges are used in a wide range of applications in the process industry. The aim is to separate the individual phases of a liquid/liquid, liquid/solid or liquid/liquid/solid system. The design of solid bowl centrifuges is based on the Σ-theory, which does not describe the separation process with a sufficiently high accuracy. This process results in numbers of experiments with high time and cost expenditure. In addition, Σ-theory only describes the stationary state and therefore do not allow the calculation of start-up processes and load changes. This chapter shows a new real-time capable numerical algorithm, which ensures a high computational efficiency and is therefore suitable for dynamic simulations of the process behavior of solid bowl centrifuges. The introduction deals with the state of the art and the existing problems concerning of the design of solid bowl centrifuges. Subsequently, material functions representing the separation properties in solid bowl centrifuges are expounded. The developed material functions are the basis for the dynamic simulation of the process behavior in solid bowl centrifuges described below. The residence time and flow conditions of the apparatus significantly influence the process behavior for semi-batch and continuous processes. The last two sections present the dynamic modeling of continuously operating decanter and semi-batch tubular centrifuges. Example simulations and comparisons to experiments validate the developed dynamic models and demonstrate the applicability for dynamic simulations.

Nomenclature

A_s	Cross section of the sediment [m]
B_{sc}	Screw pitch [m]
C	G-force [−]
D	Flow number [−]

M. Gleiss (✉) · H. Nirschl
Institute of Mechanical Process Engineering and Mechanics, Karlsruhe Institute of Technology (KIT), Karlsruhe, Strasse am Forum 8, 76131 Karlsruhe, Germany
e-mail: marco.gleiss@kit.edu

S. Heinrich (ed.), *Dynamic Flowsheet Simulation of Solids Processes*,
https://doi.org/10.1007/978-3-030-45168-4_7

$E(D)$	Residence time distribution function [−]
E	Separation efficiency [−]
$F(D)$	Residence time distribution [−]
G	Grade efficiency [−]
h	Hindered settling factor [−]
L_{cyl}	Length of the cylindrical drum [m]
L_{hel}	Length of the unrolled screw channel [m]
$\dot{m}_{\mathrm{s,i\ -\ 1}}$	Incoming mass flow of solids [kg s^{-1}]
$\dot{m}_{\mathrm{s,i}}$	Outgoing mass flow of solids [kg s^{-1}]
$\dot{m}_{\mathrm{s,sep}}$	Mass flow of separated solids [kg s^{-1}]
N	Total number of compartments [−]
n_{RZ}	Exponent Richardson and Zaki [−]
p_1	Empirical parameter for solids pressure function [Pa]
p_2	Empirical parameter for solids pressure function [−]
p_{s}	Solids pressure [Pa]
P	Product loss [−]
$q_{3,\mathrm{i}}$	Mass density distribution [m^{-1}]
Q	Volumetric flow rate [$\mathrm{m}^3\ \mathrm{s}^{-1}$]
r_1, r_2	Empirical parameters for hindered settling function [−]
R_{d}	Radius of the bowl [m]
R_{m}	Mean radius of the bowl [m]
R_{max}	Maximum radius of the sediment [m]
R_{s}	Radius of sediment surface [m]
R_{w}	Radius of the weir [m]
Re_{p}	Particle Reynolds number [−]
$\mathrm{S}_{\mathrm{dyn}}$	Normalized dynamic change [−]
t	Time [s]
T	Transport efficiency [−]
x	Particle diameter [m]
$x_{50,3}$	Mean particle diameter dependent on mass [m]
U	Volumetric Filling level [−]
U_{max}	Maximum volumetric filling level [−]
V_{hel}	Volume of the screw channel in the cylindrical part of the decanter centrifuge [m^3]
V	Volume of a compartment in the sedimentation zone [m^3]
V_{sed}	Sediment volume [m^3]
β	Screw angle [rad]
Δl	Length of a compartment [m]
Δn	Differential speed between screw and drum [rpm]
η	Dynamic viscosity [Pa s]
ϕ	Solids volume fraction [−]
$\overline{\phi}_c$	Mean solids volume fraction of the sediment [−]
ρ	Density [kg m^{-3}]
τ	Mean residence time [s]
ω	Angular velocity [s^{-1}]

Indices

0	Initial position of the particle
i	Compartment
l	Liquid
N	Total number of compartments
S	Solid
sol	Solution
tr	Transport

Abbreviations

CFD	Computational fluid dynamics
CSTR	Continuous stirred tank reactor
MPC	Model predictive control
ODE	Ordinary differential equation
PFR	Plug flow reactor
PVC	Polyvinylchloride
RTD	Residence time distribution
SRF	Single rotating frame

1 Introduction

Processes dealing with particle formation such as crystallization or precipitation, syntheses but also the fermentation of biological components usually take place in an aqueous medium [1, 2]. For better handling and transport as well as further processing of the mostly particulate valuable material, mechanical fluid separation is essential as a subsequent separation step after particle generation. Since centrifuges apply large centrifugal forces, there is a decrease of particle settling time compared to the settling in the gravity field, which reduces the process time significantly. In the field of centrifugation, a distinction is made between solid bowl and filter centrifuges. Solid bowl centrifuges have an impermeable bowl. In filter centrifuges, in contrast, the bowl is permeable for the filtrate. The particles usually remain on the filter cloth. At this point, it should be noted that this contribution is limited to the modeling of solid bowl centrifuges.

The design of solid bowl centrifuges is based on highly simplified models such as the Σ-theory [3, 4]. The Σ-theory regards the physical behavior of the material in solid bowl centrifuges as a "black box" and neglects transient phenomena, which occur due to the spin-up process or as a reaction to load changes. Additionally, Σ-theory does not consider flow conditions, settling behavior, cake formation and

sediment transport [5]. For the scale-up of solid bowl centrifuges the manufacturers use numbers of experiments on a pilot scale. This procedure is time-consuming and cost-intensive and does not allow any prediction about the dynamic process behavior [6]. For a theoretical description of the transient response of solid bowl centrifuges, it is necessary to consider flow conditions and separation behavior. A major challenge in depicting the separation process in solid bowl centrifuges arises from the fact, that particle separation depends on the residence time in the apparatus. In contrast to thickeners, the flow direction in solid bowl centrifuges results in a classification of particles along the rotor [7].

In the field of flowsheet simulation, it is important to predict the steady-state or dynamic behavior of a process plant using time-efficient mathematical models. For other applications such as Model Predictive Control (MPC) it is essential to calculate faster than real time to enable a coupling of dynamic modeling with the process control level. Mesh-based methods such as Computational Fluid Dynamics (CFD) are not suitable for flowsheet simulations [8, 9]. CFD simulations rather serve to derive parameters, that are not achievable experimentally from numerical experiments [10, 11].

The following section begins with an overview of the experimental setup to investigate material functions for the settling behavior and the cake formation process. The dynamic model for solid bowl centrifuges uses material functions for process-orientated dynamic simulations. Subsequently, different experimental methods to characterize the system and residence time behavior for decanter centrifuges are presented. Based on the investigations of material and process behavior the following section deals with the mathematical modeling of the dynamic behavior of continuously working decanter centrifuges. The comparison of dynamic simulations with pilot-scale experiments for decanter centrifuges shows the applicability of the developed numerical approach. The following section shows the development of a dynamic model for semi-continuously operating tubular centrifuges. Simulations of a tubular centrifuge on a pilot scale reveal a different process behavior of tubular centrifuges compared to decanter centrifuges. Finally, the conclusion summarizes the main results and gives a short outlook on further work.

2 Material Functions and Separation Properties

The properties of the disperse and the fluid phase such as particle size, particle shape, solid volume fraction, physicochemical properties, density of solid and liquid as well as dynamic viscosity have a significant influence on the material behavior during mechanical fluid separation [12]. Due to the large number of influencing quantities, there are no generally applicable models for the arbitrary product. Rather, it is preferable to investigate the material properties in a laboratory apparatus and to develop material functions for the theoretical description of the separation process [13]. The use of well-established laboratory equipment, such as beaker centrifuges or filters is one way to achieve this goal [14, 15]. In the case of solid bowl centrifuges,

the process behavior depends on various influencing factors for instance, the settling behavior, sediment build-up, sediment transport and mechanical dewatering [16, 17]. In the following subsection the experimental investigation of material functions for finely dispersed materials is presented in more detail.

2.1 Settling Behavior of Finely Dispersed Particles in the Centrifugal Field

The settling behavior of finely dispersed particles has a decisive influence on the separation efficiency of solid bowl centrifuges. Especially in the case of a high solid content, the particles affect each other due to an increasing hydrodynamic interaction between solid and liquid. As a result, Stokes law for particle settling is no longer valid and a correction function for hindered settling is necessary. A measuring system for determining the settling behavior of slurries is the LUMiSizer, which is an analytical centrifuge for the investigation of small product quantities of a few milliliters [15].

Figure 1a shows schematically the measuring setup within the analytical centrifuge which consists of a light source, a cuvette and a CCD sensor. The CCD sensor records the transmission versus time along the radial position of the cuvette. The integrated software calculates the settling velocity of the samples from the raw data of the transmission profiles, see right-hand side in Fig. 1. The LUMiSizer allows the simultaneous analysis of up to twelve samples. The maximum speed is $n = 1000$ rpm, which corresponds to a g-force of $C = 2320$. The hindered settling function serving to describe the settling behavior of the investigated slurry, results from the analysis of different solid volume fractions.

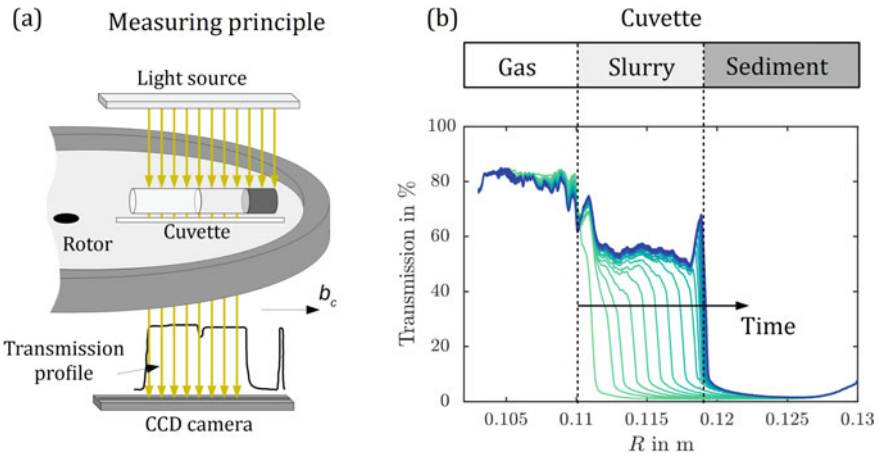

Fig. 1 Schematic representation of the measuring principle for the analytical centrifuge LUMiSizer (**a**). Temporal change of transmission along the radius of a cuvette for the product limestone (**b**)

Richardson and Zaki [18] postulate a power law based on experimental investigation for the hindered settling

$$h = (1 - \phi)^{n_{RZ}}, \tag{1}$$

for slurries consisting of monodisperse particles. For creeping flows ($Re_p < 0.1$), the exponent n_{RZ} is 4.65. The approach of Richardson and Zaki, however, is only valid for monodisperse particles and therefore represents a simplification of the real behavior of a polydisperse particle system. To investigate these, it is appropriate to measure the material function for settling behavior by means of analytical centrifugation. Often the hindered settling approach

$$h = \left(1 - \frac{\phi}{r_1}\right)^{r_2}, \tag{2}$$

of Michaels and Bolger is applied in this case to adapt to the experimental data [19]. Here, r_1 and r_2 be adapted to fit the experimental data. Figure 1 Schematic representation of the measuring principle for the analytical centrifuge LUMiSizer (a). Temporal change of transmission along the radius of a cuvette for the product limestone (b).

Figure 2 shows the normalized settling velocity related to the g-force as a function of the solids volume fraction for limestone-water suspensions with different mean particle sizes. With higher solid content the influence of hydrodynamic interactions on the particle settling increases significantly. The impact of particle size on the investigated limestone-water suspensions is also evident. There is a shift of the settling velocity towards higher values with the increase of the particle size.

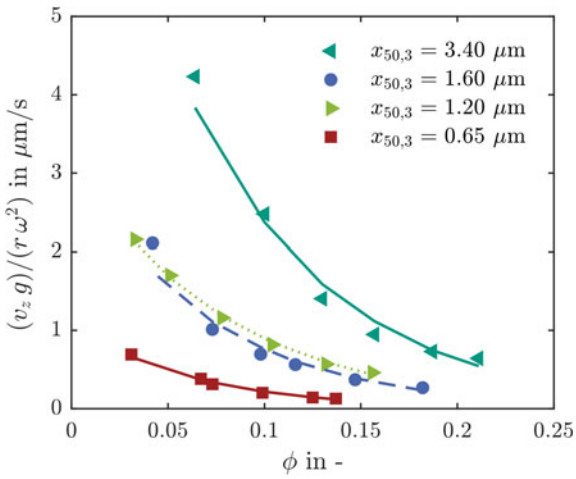

Fig. 2 Normalized settling velocity for limestone-water suspensions with for differing particle size distributions [20]

2.2 Sediment Build-up in the Centrifugal Field

Additionally to the settling behavior, sediment build-up in solid bowl centrifuges effects the separation performance. Here, the properties of the disperse phase have a huge impact on the physical behavior during the sediment formation process. Coarsely dispersed particles form an incompressible cake. In contrast, finely dispersed particles form a compressible cake. The reason for this varying behavior results from the increasing strength of interparticle forces on finely dispersed particles ($x < 10\ \mu m$).

The difficulty in describing the sediment structure of finely dispersed particles lies in the fact that the material behavior changes suddenly at the transition between suspension and sediment. Particles in a slurry move freely and hydrodynamic effects primarily influence the settling behavior. The sediment transmits normal and shear stresses inside the cake. In literature [21, 22], the gel point is defined to mark the transition between particle settling and cake compression. It is the solids volume fraction of the top sediment layer for which the solids pressure is $p_s = 0$ Pa.

Table 1 shows the comparison of the gel point for six different particulate systems, which differ in particle size. For polyvinylchloride (PVC) and limestone 1, the gel point corresponds approximately to the solids volume fraction of the formed sediment. For both products, the impact of inertial forces is significantly great compared to particle-particle interactions. For finer particles, it is clearly visible, that the behavior is entirely different. By reducing the particle size, the influence of mass forces is neglectable and thus, as a result, the particle-particle interactions increasing remarkably. For these particulate systems, the gel point is below the maximum achievable solids volume fraction in the sediment.

Laboratory centrifuges are also suitable for characterizing the sediment structure. For the experimental investigation of the cake heights for low pressures in the range of up to $p_s = 10^5$ Pa the analytical centrifuge LUMiSizer is used. Here, Usher et al. [23] show a measuring procedure for the investigation of compressible saturated sediments. The solids pressure can be derived as a function of the solids volume fraction for the equilibrium state. The analytical centrifuge starts at low rotational speed and centrifuges the sample to the equilibrium state. If there is no change in the transmission profile, the next step is to increase the rotational speed. Afterwards, the

Table 1 Comparison of the gel point for different particulate systems

Product	$x_{50,3}$ in µm	ϕ_{gel} in −
PVC	30	0.48
Limestone 1	80	0.48
Limestone 2	3.4	0.23
Limestone 3	1.6	0.16
Limestone 4	1.2	0.09
Limestone 5	0.7	0.07

sediment is centrifuged to the equilibrium for the next speed. Each measuring point represents a solids volume fraction and a solids pressure.

At this point, it should be mentioned that the filling level of the cuvette and the maximum speed are limiting factors measuring the compression behavior of the sediment in the LUMiSizer. However, solid bowl centrifuges achieve significantly higher solids pressures of up to $p_s = 10^6$ Pa. Experimental investigation for higher rotational speeds is therefore necessary. Hermle cooling centrifuge type ZK630 achieves larger centrifugal accelerations of up to $C = 6000$ and therefore serve to investigate of higher solids pressures. Special bucket systems allow the analysis of the cake formation based on investigations of the equilibrium state by gravimetric measurements.

Figure 3 illustrates the solids pressure as a function of the normalized solids content which is the ratio of solids volume fraction and gel point, for four limestone fractions with mean particle sizes of $x_{50,3} = 0.65$ µm, $x_{50,3} = 1.2$ µm, $x_{50,3} = 1.6$ µm and $x_{50,3} = 3.4$ µm. Comparing the individual limestone fractions, it is noticeable that there is a shift in the curves with a reduction of particle size. The finer the particles, the more compressible is the formed sediment. For an average particle size of $x_{50,3} = 3.4$ µm the sediment at $p_s = 10^5$ Pa compresses up to a maximum of 2.3 times compared to gel point. For the limestone with a mean size of $x_{50,3} = 0.65$ µm, the sediment has a higher compressibility. For a solids pressure of $p_s = 10^6$ Pa cake compresses up to a maximum of six times compared to the gel point.

To transfer the experimental data to the dynamic model for solid bowl centrifuges, a power law by Green et al. [24] serves to adapt the experimental data. Solids pressure

$$p_s = p_1 \left[\left(\frac{\phi}{\phi_{gel}} \right)^{p_2} - 1 \right], \tag{3}$$

is a function of the solids volume fraction. p_1 and p_2 represent empirical parameters. Furthermore, sediment flow and sediment transport have a significant influence on the process behavior of solid bowl centrifuges. The pores of finely dispersed sediments have a very high capillary pressure. Therefore, the undersaturation of the sediment is not possible. Rather, a pasty, liquid-saturated sediment formed by finely dispersed particles has a non-Newtonian rheology [25, 26]. Due to the dependency of

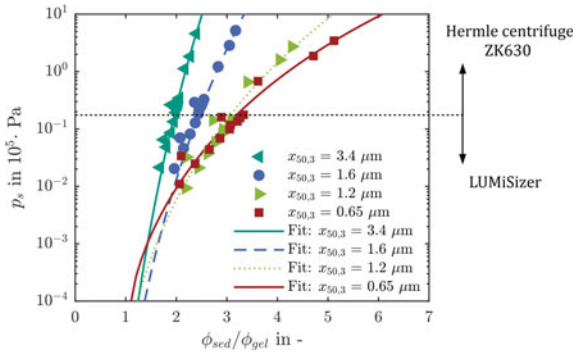

Fig. 3 Comparison of solids pressure as a function of normalized solids volume fraction for four finely dispersed limestone-water suspensions [20]

the existing yield point on the solids pressure, the experimental determination of the rheological material properties is very challenging. Here, the yield point increases with the reduction of porosity. Moreover, the material is either dilatant or shear thinning. Since no measurement methods are currently available to determine the rheological material properties, an adjusting parameter is defined to describe the sediment transport. The influence of this parameter is shown in more detail in Sect. 4.2.

3 System and Residence Time Behavior

In addition to the material behavior of the suspension, the flow conditions have a considerable influence on the operation of solid bowl centrifuges. For tubular and decanter centrifuges, for example, the residence time limits particle separation. Knowledge about the residence time behavior is therefore essential for the design of these centrifuge types. One possibility for the description of the flow conditions is the determination of the residence time and system behavior by means of experimental or numerical investigations. This approach considers the integral output response after a sudden change at the inlet. Dead zones and vortices create a dispersion in the system. This means that a step response at the outlet does not follow from a step change at the inlet.

The left-hand side in Fig. 4 shows exemplarily the residence time behavior of a density distribution and a sum distribution as a function of the flow number D. The ratio of measuring time and mean residence time τ yields the flow number. The sum distribution $F(D)$ is integral value of the density distribution $E(D)$:

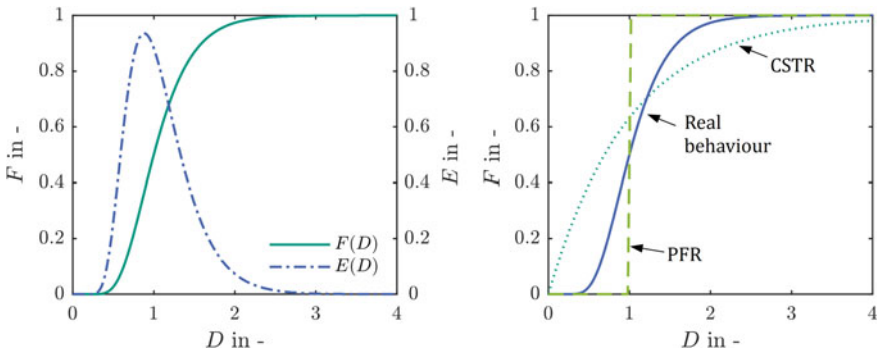

Fig. 4 Left: exemplary residence-time distribution function $E(D)$ and cumulative distribution curve $F(D)$ as a function of flow number. Right: cumulative distribution function for three different flow types [20]

$$F(D) = \int_0^D E(D)dD. \tag{4}$$

For the mean residence time $D = 1$, the residence time spectrum reaches its maximum and the residence time distribution reaches the mean value.

The right side in Fig. 4 illustrates the comparison of the real residence time behavior with an ideal plug flow reactor (PFR) and a continuous stirred tank reactor (CSTR). PFR modeling assumes, that the flow is uniform and there is no exchange of forces along the cross-section. This results in a sudden change of the residence time behavior after reaching the mean residence time. CSTR modeling supposes no gradients in the apparatus and the change occurring immediately at the output. This leads to a broad sum distribution with high axial dispersion. Real processes generally differ significantly from the performance of a PFR and CSTR, see Figs. 1 and 4, because the axial dispersion depends on the flow conditions. Dead zones and back-mixing are present inside centrifuges. Consequently, the real residence time behavior of a process differs considerable from ideal behavior.

Several methods are suitable for determining the real residence time behavior, see Fig. 5. The characterization of the residence time behavior for decanter centrifuges has been examined applying three methods: experimental residence time measurement, investigation of the system behavior and CFD simulations of a tracer transport. Experimental residence time measurements are based on the transport of a tracer material through the apparatus. In this work, saturated sodium-chloride solution is in use with a mass fraction of 2 wt%. This corresponds to a density of the saturated solution of $\rho_{\mathrm{sol}} = 1012$ kg m^{-3}. For the determination of the real residence time behavior of the centrifuge it plays an important role, that there is only a neglectable difference in density between the liquid and the tracer. Otherwise segregation of the two fluids occur due to the acting g-force. At this point it should be

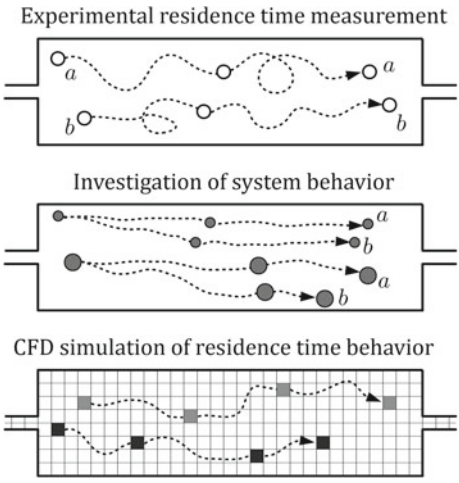

Fig. 5 Comparison of the investigated three different methods to determine the residence time distribution for solid-bowl decanter centrifuges [20]

noted, that experimental residence time measurement only considers a machine filled with liquid.

The second method is the determination of the system behavior for the same lab-scale decanter centrifuge. Here, the particle size or the solids volume fraction is changed at the inlet to investigate the response of the machine to the load change applied. The third method applies CFD simulations in combination with a passive tracer transport.

The left-hand side of Fig. 6 shows the response to an abrupt change of the solids volume fraction at the inlet. After reaching the steady state, the solids volume fraction was determined at time $t = 0$ s switching the installed three-way valve from tank 1 with $\phi_{\text{in}} = 0.02$ to tank 2 with $\phi_{\text{in}} = 0.03$. A time-delayed system behavior can be derived from the experiments, which results from the present flow conditions and the existing hold-up in the decanter centrifuge. As a consequence of the growing solids volume fraction at the inlet the momentum exchange between solid and liquid increases significantly.

For a better comparison of the temporal behavior during the abrupt change of the solids volume fraction, the right-hand side of Fig. 6 exhibits the normalized dynamic change as a function of the flow rate. The normalized dynamic change

$$S_{\text{dyn}} = \left| \frac{\phi_{\text{start}} - \phi(t)}{\phi_{\text{end}} - \phi_{\text{start}}} \right|. \tag{5}$$

describes the temporal change between the initial and final state of the sudden change at the inlet. Thus, the values range between $S_{\text{dyn}} = 0$ and $S_{\text{dyn}} = 1$. This enables the comparison between individual measurements as well as the experimental and numerical residence time investigation. The comparison of the normalized dynamic change shows an approximately identical behavior for the three investigated methods, which is represented by the s-shaped curve on the right-hand side in Fig. 6.

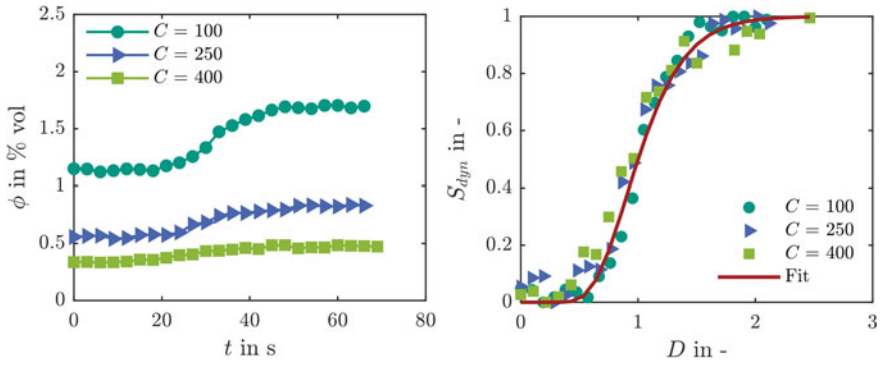

Fig. 6 Left: temporal change of solids volume fraction at the overflow dependent on g-force (C = 100, C = 250, C = 400) for a decanter centrifuge type MD80 from Lemitec GmbH. Right: normalized dynamic change as a function of flow number for the investigated change of solids volume fraction [6]

The third method to determine the residence time behavior is based on CFD simulations in combination with a transport equation taking into account the dispersion of a tracer by a passive scalar [27]. Modeling a passive scalar using a transport equation requires that the tracer has the same physical properties as the fluid. Thus, there is no cross-exchange due to a density difference.

The CFD simulations assume, that the screw rotates at the same speed as the bowl. Thus, a SRF describes the influence of centrifugal and Coriolis force. Additionally, a stationary flow is expected for the CFD simulations. Moreover, at the beginning there is no tracer in the centrifuge ($F = 0$). The step change to $F = 1$ simulates the injection of the tracer into the lab-scale decanter centrifuge. By specifying $F = 1$ at the inlet, the residence time behavior results directly from the tracer concentration at the overflow.

Figure 7 shows schematically the procedure for determining the residence time behavior using CFD simulations. The investigation of the residence time behavior based on CFD simulations is currently only applicable for a decanter centrifuge filled with liquid. The inclusion of the real behavior during operation requires the consideration of the sediment build-up and sediment transport. Currently, however, no meaningful models are available that allow CFD simulations in combination with sediment transport in decanter centrifuges. Hammerich et al. [11] show a first approach for the description of the rheological behavior for finely dispersed sediment using the example of tubular centrifuge.

The left side in Fig. 8 compares the three methods investigated for the step change of solids volume fraction, the tracer experiment and the CFD simulation. Here, it can be summarized that there is good agreement between the three methods and the residence time behavior also influences the dynamic behavior of the lab-scale decanter centrifuge. The reason for this is that the temporal change of the solids volume fraction at the overflow after a sudden change at the inlet depends on the

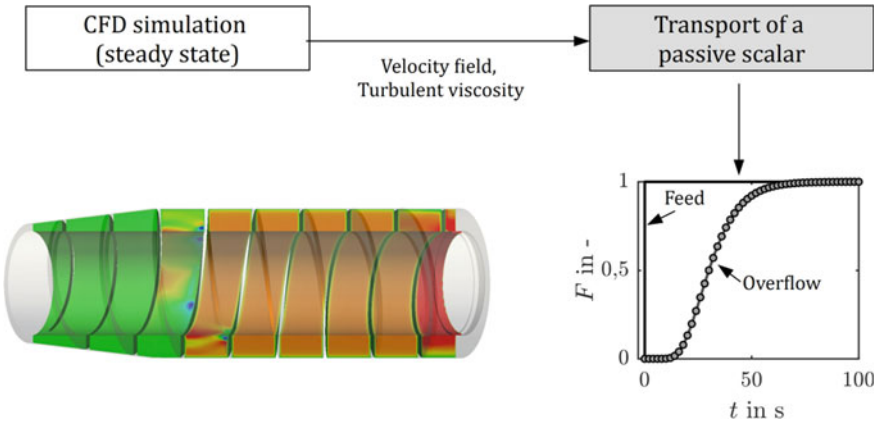

Fig. 7 Schematic representation of the CFD simulations to determine the residence time behavior of a lab-scale decanter centrifuge type MD80. Reprinted with permission from [20]

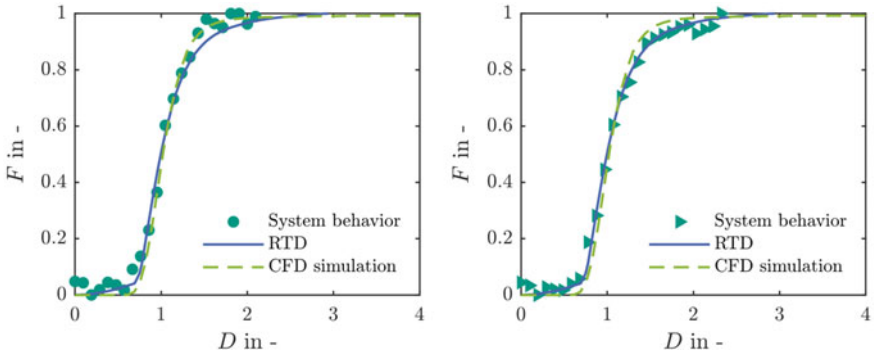

Fig. 8 Left: comparison between tracer experiment, tracer simulation and system behavior for a stepwise change of solids volume fraction at the inlet. Right: comparison between the tracer experiment, tracer simulation and stepwise change of particle size distribution at the feed [20]

flow conditions inside the machine. The rotor and the screw body limit the flow domain. No slip conditions apply to all walls. This results in the formation of a flow profile. In addition, the turbulent flow generates vortices leading to an increased momentum exchange. The left-hand side in Fig. 8 compares the residence time and the system behavior for the abrupt change of the particle size distribution at the inlet. It is apparent that three methods show a good agreement. In the next step, the system behavior is used for the dynamic modeling of decanter centrifuges.

4 Dynamic Modeling of Decanter Centrifuges

Decanter centrifuges are used in many sectors of the process industry for the separation of solids and liquids. They consist of a cylindrical-conical bowl, a screw conveyor and the feed pipe. A schematic representation of a decanter centrifuge is shown in Fig. 9. The suspension flows axially into the centrifuge where it is pre-accelerated at the transition between the cylindrical and conical part. The slurry flows along the formed channel in the screw body towards the overflow. The solid material, which usually has a higher density, settles in towards the inner wall of the bowl and is deposited there as liquid-saturated sediment. For a countercurrent decanter centrifuge, the screw body transports the sediment within the conical part of the machine.

So far, the known theoretical models for decanter centrifuges neglect the dynamic behavior. However, this occurs in decanter centrifuges during the spin-up process or as a reaction to load changes at the inlet. In the following, the dynamic modeling of countercurrent decanter centrifuges by means of the interconnection of individual compartments (index i) is presented. Figure 9 illustrates schematically the compartment model for the cylindrical part of a decanter centrifuge. The sedimentation zone and the sediment zone define two areas with differing physical behavior for the

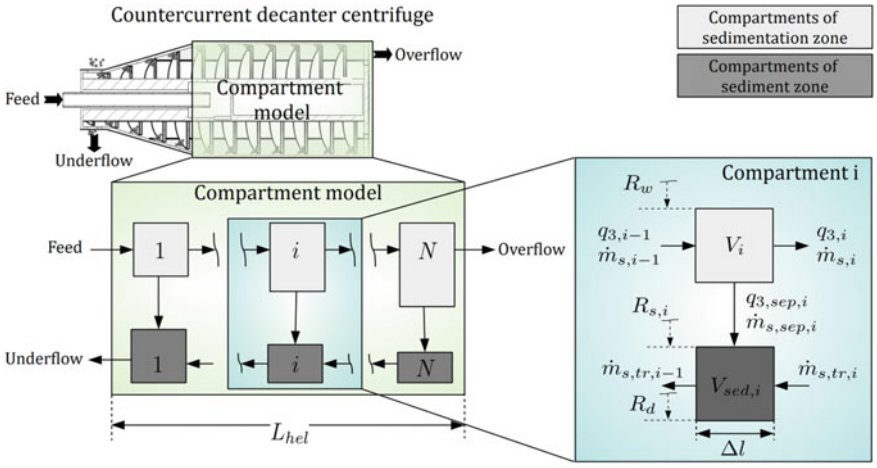

Fig. 9 Schematic representation of the compartment model for countercurrent decanter centrifuges [6]

mathematical modeling of settling behavior and sediment build-up. The linking of the individual compartments characterizes the dynamic behavior of the apparatus. This approach is also well known from chemical reaction engineering as tank-in-series model. The serial connection of ideally back-mixed compartments maps the residence time behavior of the apparatus.

The right-hand side in Fig. 9 depicts the incoming $(\dot{m}_{\mathrm{s,i-1}})$ and outgoing $(\dot{m}_{\mathrm{s,i}})$ mass flow of solids. Additionally, the incoming $(q_{3,\mathrm{i-1}})$ and outgoing $(q_{3,\mathrm{i}})$ mass density distribution are shown, which consider the change of particle size for each compartment (index i). In contrast to the well-known Σ-theory, the solid mass flow, and the particle size distribution change locally within the machine. This enables a process-related description of the classification process for decanter centrifuges.

Due to the centrifugal separation of the particles within the apparatus, the approach considers the partial removal of particle fractions for each compartment. The sediment zone then takes the separated solid mass flow $(\dot{m}_{\mathrm{s,sep,i}})$ into account for the calculation of the sediment formation.

Furthermore, sediment transport occurs in decanter centrifuges, which influences significantly the filling process. The numerical approach considers the physical behavior during the sediment transport by an incoming $(\dot{m}_{\mathrm{tr,i}})$ and outgoing $(\dot{m}_{\mathrm{tr,i-1}})$ sediment mass flow in the mass balance of the sediment in each compartment. In the case of decanter centrifuges, the screw conveyor inside the rotating bowl prevents the flow of the slurry in axial direction. In fact, the material flows along the formed screw channel towards the overflow. Thus, the mathematical modeling of the spatial and temporal change requires unwinding the screw channel and its discretization along the settling paths. Figure 10 shows the unwinding of the screw channel, the discretization of the sedimentation and sediment zone as well as the sediment distribution along the screw channel exemplarily for two different time steps $t_0 = 0$ s

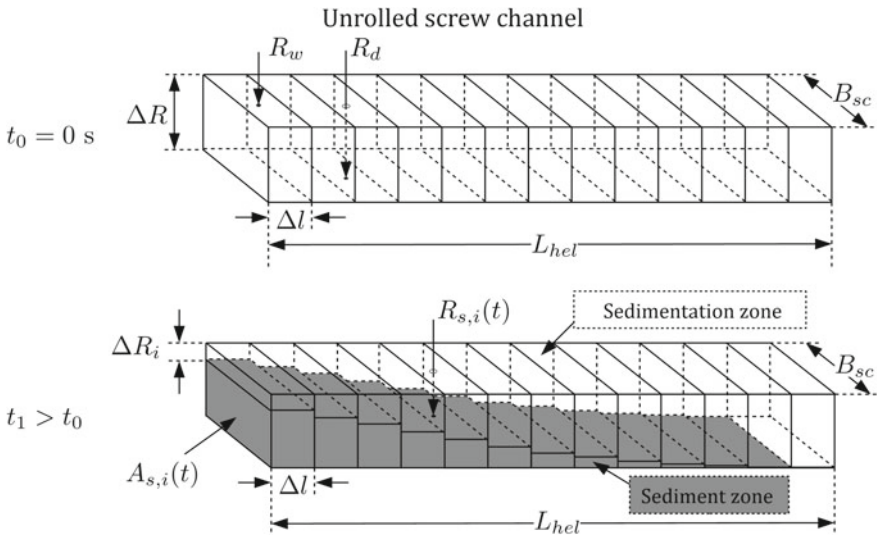

Fig. 10 Schematic representation of the unrolled screw channel, its discretization, and the sediment distribution for a countercurrent decanter centrifuge at two different time steps $t_0 = 0$ *s* and $t_1 > t_0$ [20]

and $t_1 > t_0$. The dynamic model considers the influence of the sediment build-up on the residence time behavior. In addition, the algorithm calculates the radial position of the sediment surface $R_{\mathrm{s,i}}(t)$ from the volume of the sediment $V_{\mathrm{sed,i}}$ for each compartment (index i). At the start time, different parameters such as the radius of the weir R_{w}, the radius of the drum R_{d}, the screw pitch B_{sc} and the length of the unrolled screw L_{hel} define the calculation domain.

4.1 Mathematical Modeling of the Sedimentation Zone

The sedimentation zone comprises the transport of the slurry in direction of the overflow and for the particle settling towards the inner bowl wall. For the mathematical description of the physical behavior mentioned, a series of equations are mandatory. The solids mass balance

$$\frac{dm_{\mathrm{s,i}}}{dt} = \dot{m}_{\mathrm{s,i-1}} - \dot{m}_{\mathrm{s,i}} - \dot{m}_{\mathrm{s,sep,i,}} \tag{6}$$

is applied to calculate the accumulation of solids $\frac{dm_{\mathrm{s,i}}}{dt}$ for each time step and compartment i. Here, $\dot{m}_{\mathrm{s,i-1}}$ is the incoming mass flow of solids, $\dot{m}_{\mathrm{s,i}}$ is the outgoing mass flow of solids and $\dot{m}_{\mathrm{s,sep,i,}}$ is the mass flow of separated solids. The mass flow of separated solids is calculated as the product of incoming solids mass flow and separation efficiency $E_{\mathrm{i}}(t)$:

$$\dot{m}_{\mathrm{s,sep,i}} = E_i(t) \cdot \dot{m}_{\mathrm{s,i-1}}. \tag{7}$$

The separation efficiency is an integral measure to describe the separation performance of a process and can be calculated by integrating the product of the mass density distribution function $q_{3,\mathrm{i-1}}(x,t)$ entering a compartment and grade efficiency $G_\mathrm{i}(x,t)$ over the entire particle size range $x_{\min} \leq x \leq x_{\max}$:

$$E_\mathrm{i}(t) = \int_{x_{\min}}^{x_{\max}} G_i(x,t) q_{3,\mathrm{i-1}}(x,t) dx. \tag{8}$$

Inserting Eq. (7) in (6) yields the equation for the solids mass in compartment with in the sedimentation zone:

$$\frac{dm_{\mathrm{s,i}}}{dt} = \dot{m}_{\mathrm{s,i-1}} \left(1 - E_\mathrm{i}(t) - \frac{\dot{m}_{\mathrm{s,i}}}{\dot{m}_{\mathrm{s,i-1}}} \right). \tag{9}$$

To convert the mass balance into a volume balance, the solid mass and the solid mass flow are converted into the volume and the volume flow rate. The volume balance for the compartment (index i) of the sedimentation zone

$$\frac{d\phi_\mathrm{i}}{dt} = Q_{\mathrm{i-1}} \phi_{\mathrm{i-1}} \left(1 - \int_{x_{\min}}^{x_{\max}} G_\mathrm{i}(x,t) q_{3,\mathrm{i-1}}(x,t) dx - \frac{Q_\mathrm{i} \phi_\mathrm{i}}{Q_{\mathrm{i-1}} \phi_{\mathrm{i-1}}} \right), \tag{10}$$

follows by inserting the solid mass $\left(m_{\mathrm{s,i}} = \rho_\mathrm{s} \phi_\mathrm{i} V_\mathrm{i}\right)$, the solid mass flow $\dot{m}_{\mathrm{s,i}} = \rho_\mathrm{s} \phi_\mathrm{i} Q_\mathrm{i}$ and Eq. (8) in (10). A constant volume (V_i) and ideal backmixing in the compartment is assumed to solve the ordinary differential equation (ODE) in Eq. (10). In addition, the separation process depends on the change in the particle size distribution along the screw channel. The change in the particle size distribution for the compartment with index i is as follows:

$$\frac{d\left[m_{\mathrm{s,i}} q_{3,\mathrm{i}}(x)\right]}{dt} = \dot{m}_{\mathrm{s,i-1}} q_{3,\mathrm{i-1}}(x) - \dot{m}_{\mathrm{s,i}} q_{3,\mathrm{i}}(x) - \dot{m}_{\mathrm{s,sep,i}} q_{3,\mathrm{sep,i}}(x). \tag{11}$$

Here, $\dot{m}_{\mathrm{s,i-1}} q_{3,\mathrm{i-1}}(x)$ is the incoming mass flow of particles with size x, $\dot{m}_{\mathrm{s,i}} q_{3,\mathrm{i}}(x)$ is the mass flow of outgoing particles with size x and $\dot{m}_{\mathrm{s,sep,i}} q_{3,\mathrm{sep,i}}(x)$ is the mass flow of separated particles with size x. For further consideration, the accumulation term in Eq. (11) is neglected. The assumption is made to calculate the mass density distribution of the separated solids

$$q_{3,\mathrm{sep,i}}(x,t) = q_{3,\mathrm{i-1}}(x,t) \frac{G_\mathrm{i}(x,t)}{E_\mathrm{i}(t)}, \tag{12}$$

and the mass density distribution of the outgoing stream

$$q_{3,\mathrm{i}}(x,t) = q_{3,\mathrm{i}-1}(x,t)\frac{(1-G_{\mathrm{i}}(x,t))}{(1-E_{\mathrm{i}}(t))}. \tag{13}$$

The unknown variables of the presented equations are the grade efficiency and the volume of a compartment (index i). For decanter centrifuges, the grade efficiency depends on the material properties, the centrifuge geometry and the process conditions. Gleiss et al. [6] show a shortcut model based on a grade efficiency function

$$G_{\mathrm{i}}(x,t) = \frac{R_{\mathrm{s,i}}(t)}{R_{\mathrm{s,i}}(t)-R_{\mathrm{w}}}\left\{1-exp\left[-\frac{(\rho_{\mathrm{s}}-\rho_{\mathrm{l}})h(\phi)x^2\omega^2}{18\eta_{\mathrm{l}}}\frac{B_{\mathrm{sc}}\left(R_{\mathrm{s,i}}(t)-R_{\mathrm{w}}\right)\Delta l}{Q_{\mathrm{i}-1}}\right]\right\} \tag{14}$$

to predict temporal and spatial changes along the screw channel of a decanter centrifuge as a function of the parameters described previously. Here, ρ_{s} is solids density, ρ_{l} is liquid density, η_{l} is the dynamic viscosity of the liquid, x is the particle size, ω is the angular velocity, B_{sc} is the screw pitch and Δl is the length of a compartment for the unrolled screw channel. The volume of the sedimentation zone (in a compartment i) is calculated as follows:

$$V_{\mathrm{i}} = \left(R_{\mathrm{s,i}}(t)-R_{\mathrm{w}}\right)\Delta l\, B_{\mathrm{sc}}. \tag{15}$$

4.2 Mathematical Modeling of the Sediment Zone

After particle separation, the material accumulates on the inner wall of the bowl as liquid-saturated sediment. The sediment structure depends on the separated solids and on the sediment transport. Therefore, it is essential to consider the physical behavior for the modeling of the process behavior. For this reason, this subsection deals with the mathematical modeling of the temporal and spatial changes in sediment formation. In this case, it is assumed that the maximum compaction of the sediment formed by finely disperses particles is present at the transition between the cylindrical and conical part. As a result, the conical part in the dynamic model is neglected. The description of the accumulation of solids in the centrifuge requires a mass balance of solids for each compartment (i = 1, …, N):

$$\frac{dm_{\mathrm{s,sed,i}}}{dt} = \dot{m}_{\mathrm{s,tr,i}} + \dot{m}_{\mathrm{s,sep,i}} - \dot{m}_{\mathrm{s,tr,i}-1}. \tag{16}$$

Here, $m_{\mathrm{s,sed,i}}$ is the accumulated solid mass, $\dot{m}_{\mathrm{s,tr,i}}$ is the solid mass flow transported into the compartment, $\dot{m}_{\mathrm{s,tr,i}-1}$ is the solid mass flow transported out of the compartment. Both mass flows occur because of the relative motion between bowl and screw conveyor. For the direct calculation of the sediment volume, the solids mass balance is converted into a volume balance.

$$\frac{dV_{\mathrm{s,sed,i}}}{dt} = Q_{\mathrm{s,tr,i}} + \mathrm{Q}_{\mathrm{s,sed,i}} - Q_{\mathrm{s,tr,i-1}}. \tag{17}$$

$Q_{\mathrm{s,tr,i}}$ is the flow rate of solids which is transported into the compartment, $Q_{\mathrm{s,tr,i-1}}$ is the volume flow rate of solids which is transported out of the compartment and

$$Q_{\mathrm{s,sed,i}} = \phi_{\mathrm{i-1}} Q_{i-1} E_i(t), \tag{18}$$

is the volume flow rate of separated solids. The volume flow rate of solids transported by the screw conveyor system is described as follows:

$$Q_{\mathrm{s,tr,i}} = \overline{\phi}_{c,i} A_{s,i} \cdot \frac{T B_{sc} \Delta n}{\sin(\beta)}. \tag{19}$$

Here, $\overline{\phi}_{\mathrm{c,i}}$ designates the mean solids volume fraction of the cake, $A_{\mathrm{s,i}}$ is the cross-section of the cake, T is the transport efficiency, β is the screw angle and Δn is the differential speed between screw conveyor and drum. The transport efficiency ($0 \leq T \leq 1$) is unknown and must be derived from experiments on a laboratory decanter centrifuge. $T < 1$ applies to the transport efficiency as friction and sliding occur during sediment transport. The cross-sectional area of the sediment

$$A_{s,i}(t) = B_{sc}\big(R_d - R_{s,i}(t)\big), \tag{20}$$

is calculated from the area of a rectangle with the width of the screw pitch and the difference between drum radius and the radius of the sediment surface. The latter results from the volume of the sediment in the compartment with index i:

$$R_{s,i}(t) = R_d - \frac{V_{\mathrm{sed,i}}(t)}{B_{sc} \Delta l}. \tag{21}$$

Furthermore, the length of the unrolled screw is required for the calculation of the sedimentation zone:

$$L_{\mathrm{hel}} = \frac{L_{cyl}}{B_{sc}} \cdot \left[(2\pi R_m)^2 + B_{sc}^2\right]^{0.5}. \tag{22}$$

The length of the unrolled screw is necessary to calculate the total volume of the cylindrical drum:

$$V_{\mathrm{hel}} = L_{hel} B_{sc} (R_d - R_w). \tag{23}$$

The total volume of the cylindrical drum is used here to predict the temporal change of volumetric filling level during the separation process. Furthermore, the dynamic model is based on the assumption that no sediment can grow out of the calculation area. The maximum radial position of the sediment is calculated and compared with the actual radial position of the sediment surface for each time step:

$$R_{\max} = R_{\mathrm{d}} - U_{\max}(R_{\mathrm{d}} - R_{\mathrm{w}}). \tag{24}$$

It is assumed that a maximum filling degree of $U_{\max} = 0.95$ occurs in decanter centrifuges [28]. The reason for this behavior is that a fast-flowing layer forms on the sediment surface which results in equilibrium between settling and lift of particles. For a detailed description of the dynamic modeling of the cake compression behavior of finely disperse particles, please refer to Gleiss [20].

4.3 *Validation of the Dynamic Model for Decanter Centrifuges*

This subsection shows selected results for the experimental validation of the dynamic model for a pilot-scale decanter centrifuge. The basis of dynamic simulations is the mathematical modeling presented in Sects. 4.1 and 4.2. Limestone-water and PVC-water slurries were used for the validation trials of the presented approach for decanter centrifuges on a lab and pilot scale. Table 2 shows the geometric parameters of the lab-scale and pilot scale decanter centrifuges investigated here.

Figure 11 shows the influence of the total number of compartments N on the transient behavior of the solids volume fraction at the overflow. An exemplary case with the simulation setup $Q = 30\ \mathrm{l{\cdot}h^{-1}}$, $C = 500$ and $\Delta n = 5\,\mathrm{rpm}$ illustrates the temporal change of the solids volume fraction on the left-hand side. After the spin-up process which ends after $t = 150\,\mathrm{s}$, the simulation results reveal a steady behavior. At $t = 250\,\mathrm{s}$, the solids volume fraction changes abruptly from $\phi_{\mathrm{in}} = 2\ \%\,\mathrm{vol}$ to $\phi_{\mathrm{in}} = 3\ \%\,\mathrm{vol}$ at the inlet. The results indicate that the reaction of the machine to this load change occurs time-delayed at the overflow, which has already been described in Sect. 3. The total number of compartments N has an influence on both the start-up process and the simulated load change. The reason is the reduction of the axial dispersion with the increase of N. The influence of the total number of compartments on the normalized dynamic change is depicted the right-hand side of Fig. 11.

An important parameter for the dynamic modeling of decanter centrifuges is the transport efficiency T, which describes the transport behavior of the formed sediment. Since the sediment build-up has a decisive influence on the process behavior of

Table 2 Geometric parameters of the decanter centrifuges investigated

Parameter	Lab-scale decanter (m)	Pilot scale decanter (m)
Length cylindrical bowl	0.18	0.98
Weir radius	0.034	0.104
Bowl radius	0.04	0.14
Screw pitch	0.025	0.125

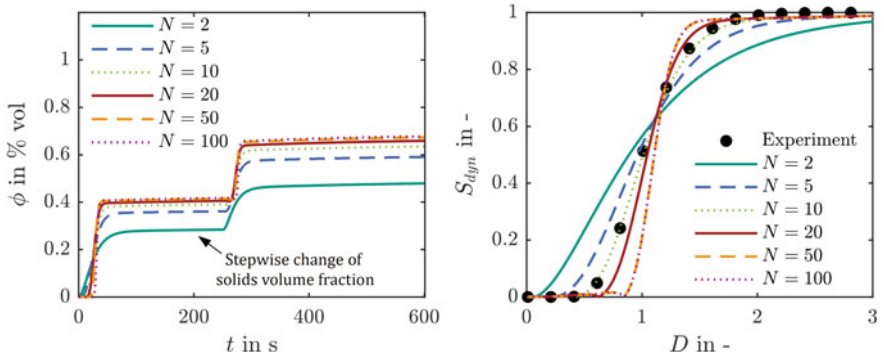

Fig. 11 Left: transient behavior of solids volume fraction at the overflow. Right: simulation for the normalized dynamic change as a function of flow number. Both diagrams show the influence of the total number of compartments N on the dynamic and residence time behavior. Simulations performed for a lab scale decanter centrifuge type MD80 at $Q = 30\ \mathrm{lh}^{-1}$, $C = 500$ and $\Delta n = 5$ rpm [20]

decanter centrifuges, it is important to know the effect of this parameter to predict separation with a good accuracy. Therefore,

Figure 12 demonstrates the influence of transport efficiency on the solids volume fraction in the overflow (left) and underflow (right). The simulation setup is based on pilot scale experiments with $Q = 500\ \mathrm{m}^3\ \mathrm{h}^{-1}$, $\phi_{\mathrm{in}} = 0.15$ and $\Delta n = 15$ rpm to verify the influence of the transport efficiency on the dynamic simulation.

According to definition, the transport efficiency is between $0 < T < 1$. For small values of T, the transport is inefficient. Conversely, $T = 1$ represents an ideal transport without friction losses. The screw conveyor moves the cake during one rotation by the screw pitch. The influence of transport efficiency on the solids

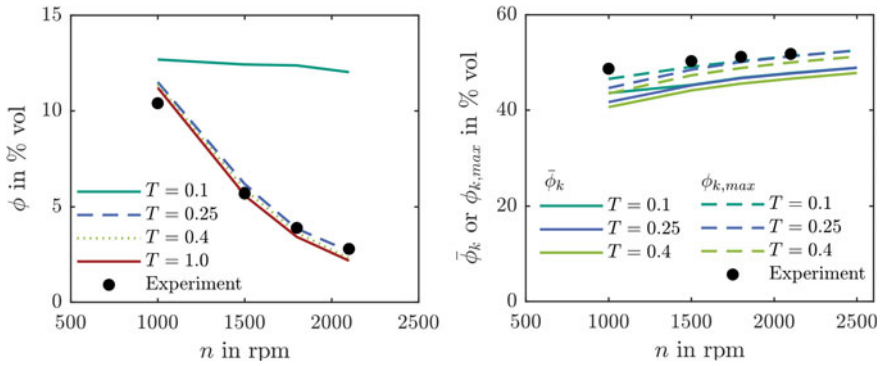

Fig. 12 Left: influence of the transport efficiency on the solids volume fraction at the overflow. Right: mean solids volume fraction at the underflow as a function of rotational speed and transport efficiency. The simulation setup is $Q = 0.5\ \mathrm{m}^3\ \mathrm{h}^{-1}$, $\phi_{\mathrm{in}} = 0.15$ and $\Delta n = 5$ rpm. Simulations performed for a pilot scale decanter centrifuge. Reprinted with permission from [20]

volume fraction in the overflow is negligible in a wide range of $0.25 \leq T \leq 1$. A clear deviation from simulation and experiment is only detectable for $T = 0.1$. For this setting, the sediment transport is inefficient and the machine fills almost completely. As a result, only a small volume is available for the separation and the solids volume fraction at the overflow increases due to the short residence time in the apparatus.

The right-hand side in Fig. 12 exhibits the impact of transport efficiency on the mean solids volume fraction $\overline{\phi}_c$ and the maximum solids volume fraction at the inner wall of the drum $\phi_{c,max}$ as a function of rotational speed. The comparison of the results points out that there is only a small influence of the transport efficiency on the solids volume fraction in the underflow. This results in only a slight shift of the curves towards a larger solids volume fraction due to the rising sediment volume.

Another field of application for decanter centrifuges is the classification of finely dispersed particles. The aim here is to adjust selectively the particle size of the valuable product. For testing the applicability of dynamic modeling, finely dispersed limestone is classified in a pilot decanter centrifuge. The following parameters serve as simulation setup: $Q = 0.5\,\mathrm{m^3\ h^{-1}}$, $\phi_{in} = 0.15$ and $\Delta n = 15$ rpm.

Figure 13 presents the mass sum distribution at the overflow for experiments and simulations for the investigated pilot decanter centrifuge as a function of rotational speed. The results indicate that there is a shift in the mass sum distribution with the increase of rotational speed. In addition, the dynamic simulations reproduce the results of the classification accurately. Thus, the dynamic model also considers the change in particle size distribution.

The sediment build-up in solid bowl centrifuges depends not only on the process conditions, but also on the material properties of the disperse phase. Additionally, the sediment build-up in decanter centrifuges is influenced by the differential speed between screw and bowl. The left side in Fig. 14 illustrates the influence of the inlet solids volume fraction on the mean solids volume fraction of the underflow. The

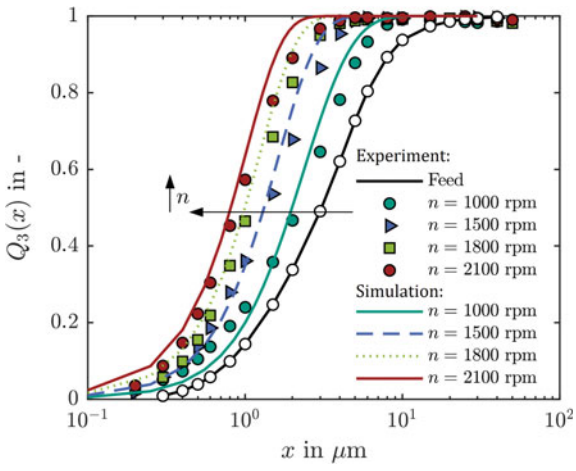

Fig. 13 Particle size distribution at the overflow for simulation and experiment dependent on rotational speed for the classification of limestone-water slurries with a pilot-scale decanter centrifuge. The simulation setup is $Q = 0.5\,\mathrm{m^3\ h^{-1}}$, $\phi_{in} = 0.15$ and $\Delta n = 5$ rpm [20]

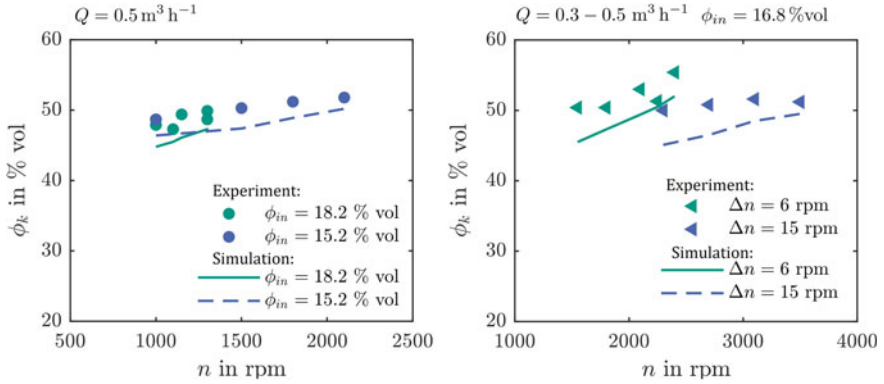

Fig. 14 Comparison of the mean solids volume fraction of the underflow dependent on rotational speed. Left: influence of feed volume fraction for finely dispersed limestone with a mean particle size of $x_{50,3} = 3.4$ µm. Right: impact of differential speed between screw conveyor and drum for a limestone-water slurry with a mean particle size of $x_{50,3} = 1.6$ µm [20]

measuring ranges overlap, which indicates that there is only a small influence of the solids volume fraction. Furthermore, the solids volume fraction of the underflow increases for higher speeds. Comparing simulation and experiment, it is easy to see that the calculation underestimates the solids volume fraction of the sediment. At this point, shear compression can lead to a denser packing of the formed saturated cakes.

The right-hand side in Fig. 14 shows the influence of differential speed (Δn) on the mean solids volume fraction at the underflow for $\Delta n = 6$ rpm and $\Delta n = 15$ rpm. The influence of the differential speed on the solids volume fraction is significantly higher for the investigated process compared to the variation of the feed solids volume fraction. This results in a denser sediment for $\Delta n = 6$ rpm at a lower speed compared to the simulation setup with $\Delta n = 15$ rpm. In addition, the simulation underestimates the experimental values for both differential speeds.

5 Dynamic Modeling of Tubular Centrifuges

Another machine type in the class of solid bowl centrifuges are fast-rotating tubular centrifuges. Due to the slim design, this centrifuge type achieves g-forces up to $C = 100000$. This makes the apparatus suitable for the separation of nanoparticles and proteins from fermentation processes. Another field of application is the defined classification of nanoparticles. Figure 15 depicts the schematic design of a tubular centrifuge. A pump delivers the mostly diluted suspension at the bottom axially into the apparatus. The geometry of the machine forms a liquid pond and a gas core. The suspension flows in axial direction and leaves the apparatus on the top. The

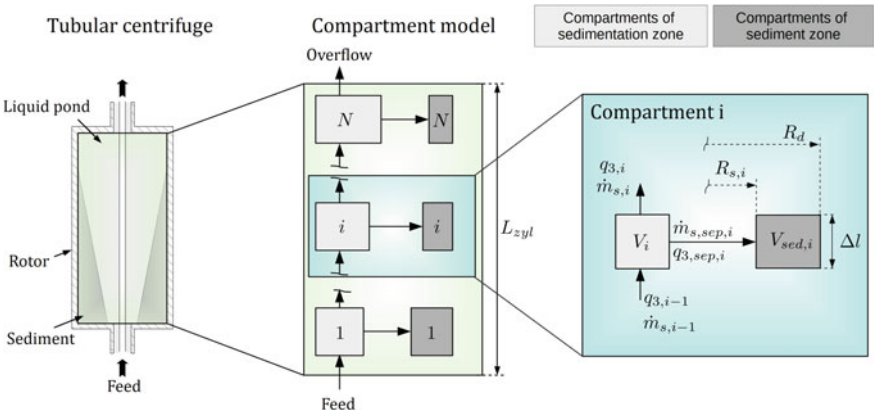

Fig. 15 Schematic representation of a tubular centrifuge, developed compartment approach and balancing of an individual compartment. Reprinted with permission from [20]

centrifugal field created by the rotation leads to particle settling in the direction of the inner rotor wall.

The basis for the mathematical modeling is the dynamic model for decanter centrifuges presented in Sect. 4.1. Sedimentation and sediment zone describe the separation of the dispersed phase and the sediment formation in the investigated tubular centrifuge. In contrast to decanter centrifuges, no sediment transport takes place. The starting point is a cohesive particle cluster that does not move because of the rheological properties of the sediment. Once the particles have been separated, the sediment remains at this axial position in the rotor. Only sediment compression in the radial direction takes place. As for decanter centrifuges, a total number of compartments (N) subdivides the inner space of the rotor. The right-hand side in Fig. 15 shows the variables modeled exemplarily for the compartment (index i). Sections 5.1 and 5.2 discuss the mathematical modeling of tubular centrifuges in more detail.

Figure 16 depicts the temporal change of sediment build-up exemplarily for three-time steps $t_0 < t_1 < t_2$. At the beginning of the dynamic simulation $t_0 = 0\,\mathrm{s}$, only liquid is present in the centrifuge. Discretization of the rotor length L_{ax} allows calculating of the sediment distribution for each time step t. After a certain time (t_2), the regions close to the inlet are almost completely filled due to the classification of the product along the rotor length. Here, simulation results from Hammerich et al. [11] show that a fast-flowing layer forms in these regions. Due to the short residence time of the slurry, no further separation occurs. Instead, the flow collects particles from the sediment surface. However, this physical behavior is not taken into account in the presented approach. If the radius of the sediment is equal or smaller than the maximum radial position of the sediment surface R_{max}, no further separation is considered in this section of the tubular centrifuge.

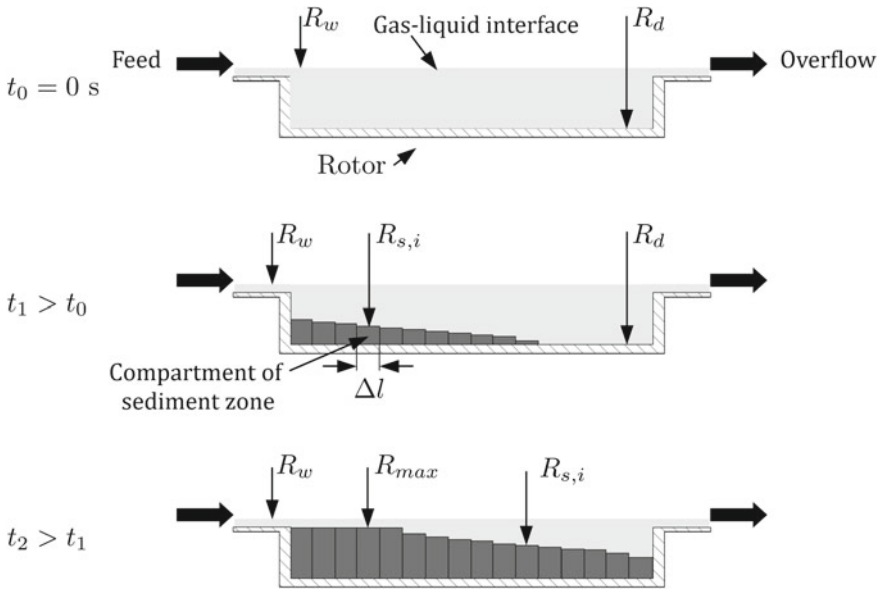

Fig. 16 Schematic representation of the temporal filling process exemplary for three-process steps $t_0 < t_1 < t_2$. Reprinted with permission from [20]

5.1 Modeling of the Sedimentation Zone

The dynamic modeling of the sedimentation zone in tubular centrifuges is based on almost the same assumptions as for decanter centrifuges. However, in contrast to decanter centrifuges, the main flow direction is axial towards the overflow. The modified residence time behavior requires to adapt the grade efficiency calculation:

$$G_i(x,t) = \frac{R_{\mathrm{s,i}}(t)^2}{R_{\mathrm{s,i}}(t)^2 - R_{\mathrm{w}}^2}\left\{1 - \left(exp\left\{-\frac{(\rho_{\mathrm{s}} - \rho_{\mathrm{l}})h(\phi)x^2\omega^2}{18\eta_{\mathrm{l}}}\frac{V_{\mathrm{i}}(t)}{Q_{\mathrm{i-1}}}\right\}\right)^2\right\}. \quad (25)$$

The main difference to the grade efficiency model for decanter centrifuges results from the differing geometry of tubular centrifuges. Neglecting the pre-acceleration zone and the overflow region, it can be described as a hollow cylinder. The volume of a compartment (index i) is calculated using the geometric dimensions of a hollow cylinder:

$$V_{\mathrm{i}}(t) = \pi\left(R_{\mathrm{s,i}}(t)^2 - R_{\mathrm{w}}^2\right)\Delta l. \quad (26)$$

The length of a compartment Δl is unknown. The ratio of the length of the cylindrical rotor L_{cyl} to the total number of compartments N describes Δl. Furthermore, the total volume of the cylindrical rotor

$$V_{\mathrm{cyl}} = \pi \left(R_{\mathrm{d}}^2 - R_{\mathrm{w}}^2 \right) L_{\mathrm{cyl}}, \tag{27}$$

is decisive for the calculation of the volumetric filling level. The mass balance for solid, liquid and particle size distribution is the same for the dynamic modeling of decanter and tubular centrifuges. At this point, it should be noted that the rotating gas core and thus the gas liquid-interphase are not considered in the dynamic model presented. Additionally, no particle breakage occurs in the feed zone of the tubular centrifuge. Moreover, the slurry rotates as a rigid body. This means that an insufficient pre-acceleration is not taken into account by the presented approach.

5.2 Modeling of the Sediment Zone

Since a tubular centrifuge is a semi-continuous apparatus, the process behavior for sediment build-up differs from that of a decanter centrifuge. Here, the solid accumulates continuously on the inner rotor wall until the apparatus is completely filled. As a result, the solids mass balance in a compartment of the sediment zone simplifies as follows:

$$\frac{dm_{\mathrm{s,sed,i}}}{dt} = \dot{m}_{\mathrm{s,sed,i}}. \tag{28}$$

The continuous supply of solids during the entire process leads to a complete filling of the rotor up to the maximum volumetric filling level theoretically. For the prediction of the radial position of the sediment surface for the compartments i = 1, …, N the solids mass balance is transformed into a volume balance of solids:

$$\frac{dV_{\mathrm{s,sed,i}}}{dt} = \mathrm{Q}_{\mathrm{s,sed,i}}. \tag{29}$$

The dynamic simulation of the sediment build-up along the axial position of the rotor allows the temporal prediction of the sediment distribution. The accumulated volume of the sediment is used to determine the radial position of the sediment surface

$$R_{\mathrm{s,i}}(t) = \left[R_{\mathrm{d}}^2 - \frac{V_{\mathrm{sed,i}}(t)}{\pi \, \Delta l} \right]^{0.5}, \tag{30}$$

for each compartment (index i). The radial position of the sediment surface is then used to calculate the volume of the sedimentation zone in Eq. (26) and thus to map the residence time behavior which deviates with process time. Stahl et al. [29] show that the sediment in tubular centrifuges only increases up to a critical volumetric filling level of $U_{\max} = 0.95$. This means that the sediment does not emerge from

the liquid pool. Rather, separated and dragged solids are in equilibrium in the fast-flowing layers of the centrifuge. The dynamic model considers the described process behavior by estimating the maximum possible radius of the sediment:

$$R_{\max} = \left[(1 - U_{\max}) \cdot \left(R_{\mathrm{d}}^2 - R_{\mathrm{w}}^2\right) + R_w^2\right]^{0.5}. \tag{31}$$

For each time step, the radial position of the sediment surface for each compartment (index i) is compared to the maximum sediment radius. For $R_{\mathrm{s,i}}(t) \geq R_{\max}$, no further particles are separated in this compartment and $G_{\mathrm{i}}(x, t) = 0$ apply for the grade efficiency. The evaluation of the temporal behavior of the separation process is based on two parameters: the product loss $P(t)$ and volumetric filling level $U(t)$. The temporal change of the volumetric filling level results from the ratio of the overall accumulated sediment volume for all compartments i = 1, …, N to the volume of the rotor:

$$U(t) = \frac{\sum_{\mathrm{i}=1}^{\mathrm{N}} V_{\mathrm{sed,i}}(t)}{V_{\mathrm{cyl}}}. \tag{32}$$

The product loss

$$P(t) = \frac{\dot{m}_{\mathrm{s,of}}}{\dot{m}_{s,\mathrm{feed}}}, \tag{33}$$

is the ratio of the solid mass flow at the overflow $\dot{m}_{\mathrm{s,of}}$ to the solid mass flow at the feed $\dot{m}_{\mathrm{s,feed}}$. The algorithm developed for the sediment formation process distinguishes between an incompressible and a compressible cake. For an incompressible cake, the porosity is not a function of the solids pressure. This results in a practically constant porosity over the sediment height. Such materials are also analyzed in beaker centrifuges to determine the porosity of the sediment for dynamic simulation. For compressible cakes, the behavior differs significantly. Here, as described in Sect. 2.2, porosity is a function of the solids pressure. For the mathematical description of the sediment build-up for compressible materials please refer to Gleiss [20].

5.3 Validation of the Dynamic Model for Tubular Centrifuges

This subsection deals with the verification of the dynamic model to predict the process behavior of tubular centrifuges. The parameters to validate the dynamic model are the product loss and the volumetric filling level. The tubular centrifuge investigated is a pilot machine of the company CEPA GmbH type GLE. Table 3 summarizes the geometric dimensions and discretization of the centrifuge.

Additionally, Fig. 17 depicts the mass distribution functions of silica with the commercial name Aerosil 200 which is applied as an initial parameter for the dynamic modeling. The mass related mean particle size is $x_{50,3} = 76$ nm.

Table 3 Summary of the key data of the investigated tubular centrifuge

Parameter	Value (m)
Rotor length	0.18
Drum radius	0.0215
Weir radius	0.0152
Number of compartments	50
Number of sediment slices	100
Number of particle classes	100

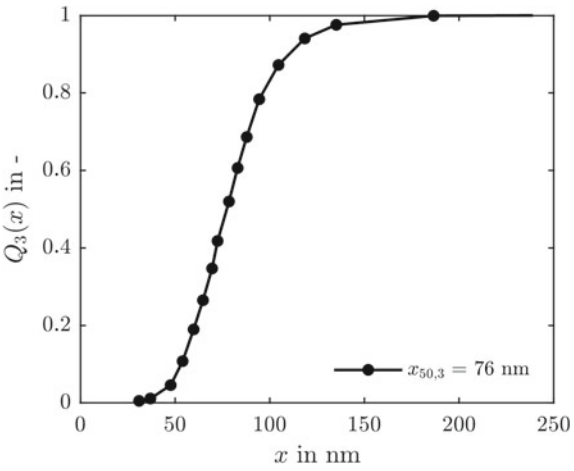

Fig. 17 Mass distribution function of silica nanoparticles with the commercial name Aerosil 200

Figure 18 shows the temporal change of product loss for the separation of silica nanoparticles, dependent on the empirical parameters of the material function for the solids pressure. The simulation setup is $Q = 0.1\ 1 \cdot \text{min}^{-1}$, $C = 19200$ and $\phi_{\text{in}} = 0.005$. The product loss changes linearly with time in the range of 1 min $< t <$ 90 min.

One of the three parameters p_1, p_2 and ϕ_{gel} was changed exemplarily for each simulation. As can be seen from Fig. 17 Mass distribution function of silica nanoparticles with the commercial name Aerosil 200.

Figure 18, the parameter variation shows a small influence on the temporal change of the product loss, but also a good agreement with the experiment.

A significant influence results for the volumetric filling level and thus for the sediment build-up in the tubular centrifuge, see Fig. 19. The variation of parameters p_1 and p_2 shifts the curve for the volumetric fill level up by about 10%. This clearly shows the influence of the compression behavior on the sediment structure and thus the importance of the meaningful prediction of the material behavior based on the methodology shown in Sect. 2.2 on a laboratory scale. Here, measurement uncertainties lead to deviations in the dynamic simulation of process behavior for tubular centrifuges and thus to deviations in the separation efficiency.

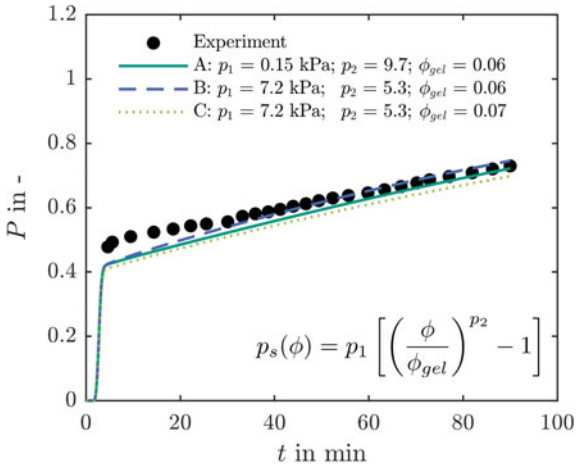

Fig. 18 Comparison of simulation und experiment for the temporal change of product loss dependent on the material properties to describe solids pressure. The simulation setup is $Q = 0.11 \cdot min^{-1}$, $C = 19.200$ and $\phi_{in} = 0.005$ [20]

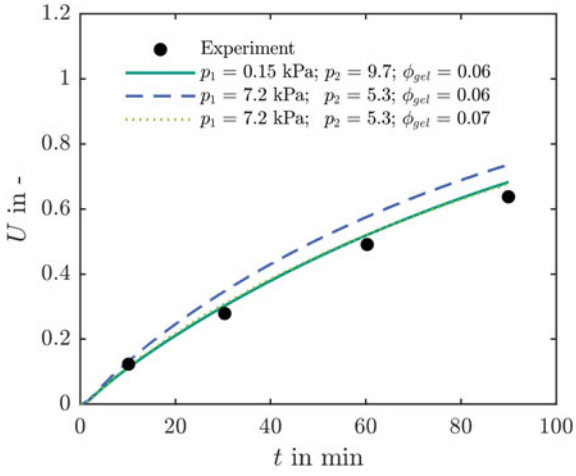

Fig. 19 Comparison of simulation and experiment for the temporal change of the filling level for the tubular centrifuge investigated dependent on the material function for the compression behavior. The simulation setup is $Q = 0.11 \cdot min^{-1}$, $C = 19200$ and $\phi_{in} = 0.005$ [20]

Figure 20 illustrates the simulated temporal change of the grade efficiency under variation of the volumetric flow rate for two different time steps $t = 10$ min and $t = 30$ min. In this case, the simulation setup is based on $C = 19200$ and $\phi_{\text{in}} = 0.005$. The results show a shift in the degree of separation with respect to the process time towards larger particle fractions, which worsens the classification.

Furthermore, the influence of the volume flow can be clearly seen. At this point there is a shift of the curves towards larger particles with the increase of the volume flow rate. The process behavior can be explained by the reduction of the residence time in the tubular centrifuge. Furthermore, the results indicate a broader grade efficiency for higher volume flow rate.

Another advantage of the dynamic model is the description of the temporal evolution of the sediment height and the sediment distribution along the rotor. As a

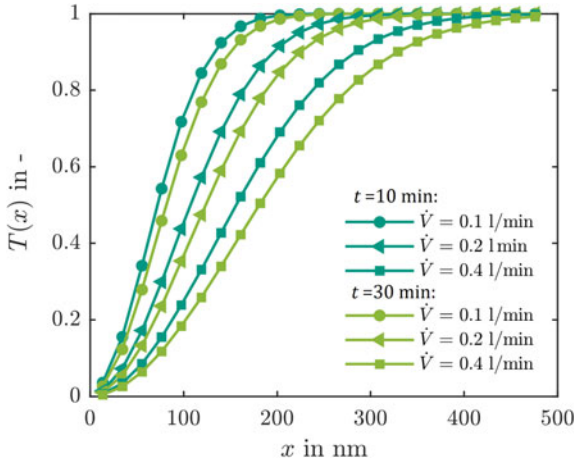

Fig. 20 Dynamic simulation of grade efficiency dependent on time and volumetric flow rate. Simulation setup is $C = 19200$ and $\phi_{\text{in}} = 0.005$ [20]

result the sediment volume can be derived for each time step. Figure 21 presents the sediment height as a function of the rotor length for $C = 9600$, $C = 28900$ and $C = 38500$. Here, the g-force refers to the bowl radius. Each iso-line corresponds to a constant time. The interval between two lines is $\Delta t = 10$ min. The results indicate deviating process behavior for the sediment build-up as a function of the volume flow. A thin sediment layer is formed in the rotor for $C = 9600$ at time $t = 90$ min. For $C = 38{,}500$ the rotor is almost completely filled. This process behavior results from the increasing amount of the separated solid for a higher g-force.

6 Conclusion

This work presents the development of two dynamic models for continuous working decanter centrifuges and semi-batch tubular centrifuges. Both models are computationally efficient and therefore suitable for dynamic flowsheet simulation and Model Predictive Control. Dynamic simulation requires material functions and the residence time behavior to predict the real process behavior with sufficient accuracy. In contrast to the Σ-theory, which carries out experiments on a pilot scale, the settling behavior and the sediment build-up were investigated sing well-established laboratory equipment. This allows a detailed numerical investigation of the process level for solid-bowl centrifuges.

Another important parameter for the description of continuous and semi-batch machines are the flow conditions, which influence the residence time of the particles. For this reason, three methods have been applied to investigate the flow conditions: the experimental residence time measurement, CFD simulations and characterization of the system behavior. The experimental data for the system behavior results from a stepwise change of particle size distribution and solids volume fraction at the feed

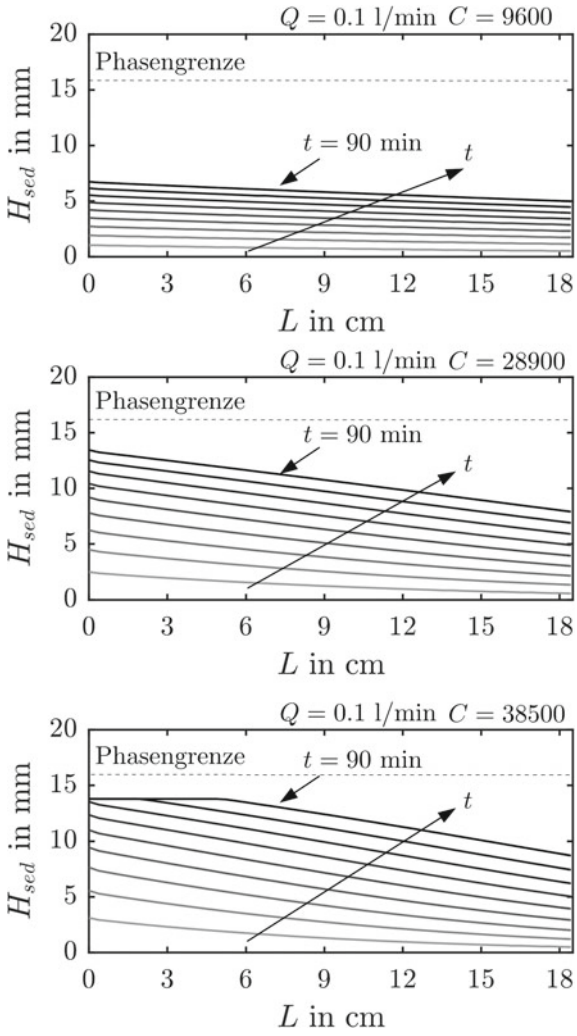

Fig. 21 Temporal change of sediment height as a function of rotor length for three g-forces $C = 9600$, $C = 28900$ and $C = 38500$. Each line represents an iso-curve for a point in time. Reprinted with permission from [20]

of a lab-scale decanter centrifuge. The results show the correlation between the residence time and the dynamic behavior. The dynamic model for decanter centrifuges is based on the interconnection of individual compartments. The numerical algorithm solves the mass balance of solids and liquid as well as for the particle size class for each compartment. Since the material behavior at the transition between suspension and sediment changes abruptly, the mathematical model divides the centrifuge into a sedimentation zone and a sediment zone. The sedimentation zone describes the dynamic behavior during the separation of the particles. Whereas the sediment zone,

considers the calculation of sediment build-up and sediment transport. The comparison of dynamic simulations with experiments for finely dispersed particle systems shows a good conformity.

Finally, the broad applicability of the developed compartment model was demonstrated by transferring the dynamic model of a continuous working decanter to semi-batch tubular centrifuges. It can be shown that the deviating process behavior of tube centrifuges is due to the sediment build-up in the rotor. In contrast to decanter centrifuges, the accumulated solids remain in the apparatus and thus reduce the flow cross-section. As a result, the residence time decreases permanently until the sediment occupies the entire rotor. The comparison with experiments for nanoscale silica also shows a good agreement between simulation and experiment for the temporal change of product loss and grade efficiency. The developed models are not only suitable for dynamic flowsheet simulation, but also for other applications. For example, it is conceivable to use dynamic models for MPC or to carry out an optimization regarding raw material or resource efficiency.

References

1. Kowalczyk, B., Lagzi, I., Grzybowski, B.A.: Nanoseparations: strategies for size and/or shape-selective purification of nanoparticles. Curr. Opin. Colloid Interf. Sci. **16**, 135–148 (2011). https://doi.org/10.1016/j.cocis.2011.01.004
2. Kanarska, Y., Lomov, I., Antoun, T.: Mesoscale simulations of particulate flows with parallel distributed Lagrange multiplier technique. Comput. Fluids **48**, 16–29 (2011). https://doi.org/10.1016/j.compfluid.2011.03.010
3. Ambler, C.M.: The evaluation of centrifuge performance. Chem. Eng. Prog. **48**, 150–158 (1952)
4. Ambler, C.M.: The theory of scaling up laboratory data for the sedimentation type centrifuge. J. Microb. Biochem. Technol. **1**, 185–205 (1959)
5. Leung, W.W.-F.: Industrial Centrifugation Technology. McGraw-Hill, New York (1998)
6. Gleiss, M., Hammerich, S., Kespe, M., Nirschl, H.: Application of the dynamic flow sheet simulation concept to the solid-liquid separation: separation of stabilized slurries in continuous centrifuges. Chem. Eng. Sci. **163**, 167–178 (2017)
7. Konrath, M., Brenner, A., Dillner, E., Nirschl, H.: Centrifugal classification of ultrafine particles: Influence of suspension properties and operating parameters on classification sharpness. Sep. Purif. Technol. **156**, 61–70 (2015)
8. Romanni Fernández, X., Nirschl, H.: A numerical study of the impact of radial baffles in solid bowl centrifuges using computational fluid dynamics. Phys. Sep. Sci. Eng. (2010)
9. Romaní Fernández, X., Nirschl, H., Fernández, X.R., Nirschl, H.: Simulation of particles and sediment behaviour in centrifugal field by coupling CFD and DEM. Chem. Eng. Sci. **94**, 7–19 (2013). https://doi.org/10.1016/j.ces.2013.02.039
10. Hammerich, S., Gleiß, M., Nirschl, H.: Modeling and simulation of solid-bowl centrifuges as an aspect of the advancing digitization in solid-liquid separation. Chemie Ing. Tech. **91**, 215–227 (2019)
11. Hammerich, S., Gleiß, M., Kespe, M., Nirschl, H.: An efficient numerical approach for transient simulation of multiphase flow behavior in centrifuges. Chem. Eng. Technol. **41**, 44–50 (2018)
12. Stahl, W.: Fest-Flüssig-Trennung Band II: Industrie-Zentrifugen, Maschinen-und Verfahentechnik. DRM Press, CH-Männedorf (2004)
13. Skinner, S.J., Studer, L.J., Dixon, D.R., Hillis, P., Rees, C.A., Wall, R.C., et al.: Quantification of wastewater sludge dewatering. Water Res. **82**, 2–13 (2015). https://doi.org/10.1016/j.watres.2015.04.045

14. Lerche, D.: Dispersion stability and particle characterization by sedimentation kinetics in a centrifugal Field. J. Dispers. Sci. Technol. **23**, 37–41 (2007)
15. Detloff, T., Sobisch, T., Lerche, D.: Particle size distribution by space or time dependent extinction profiles obtained by analytical centrifugation. Powder Technol. **174**, 50–55 (2007)
16. Anlauf, H.: Recent developments in centrifuge technology. Sep. Purif. Technol. **58**, 242–246 (2007). https://doi.org/10.1016/j.seppur.2007.05.012
17. Beiser, M., Bickert, G., Scharfer, P.: Comparison of sedimentation behavior and structure analysis with regard to destabilization processes in suspensions. Chem. Eng. Technol. **27**, 1084–1088 (2004). https://doi.org/10.1002/ceat.200403252
18. Richardson, J.F., Zaki, W.N.: Sedimentation and fluidisation: Part I. Chem. Eng. Res. Des. **75**, 82–100 (1997)
19. Michaels, A., Bolger, J.: Settling rates and sediment volumes of flocculated kaolin suspensions. Ind. Eng. Chem. Fundam. **1**, 24–33 (1962)
20. Gleiß, M.: Dynamische Simulation der Mechanischen Flüssigkeitsabtrennung in Vollmantelzentrifugen, KIT Scientific Publishing (2018)
21. Stickland, A.D.: Solid-liquid separation in the water and wastewater industries. University of Melbourne (2005)
22. Spelter, L.E., Nirschl, H., Stickland, A.D., Scales, P.J.: Pseudo two-dimensional modeling of sediment build-up in centrifuges: a compartment approach using compressional rheology. AIChE J. **59**, 3843–3855 (2013)
23. Usher, S.P., Studer, L.J., Wall, R.C., Scales, P.J.: Characterisation of dewaterability from equilibrium and transient centrifugation test data. Chem. Eng. Sci. **93**, 277–291 (2013)
24. Green, M.D., Eberl, M., Landman, K.A.: Compressive yield stress of flocculated suspensions: determination via experiment. AIChE J. **42**, 2308–2318 (1996)
25. Mladenchev, T., Tomas, J.: Modellierung der Filtrations- und Konsoldierungsdynamik von geflockten und nicht geflockten feindispersen Kalksteinsuspensionen. Chemie Ing. Tech. **76**, 1814–1818 (2004)
26. Erk, B., Luda, A.: Beeinflussung der Schlammkompression in Vollmantelzentrifugen. Chemie Ing. Tech. **75**, 1250–1254 (2003). https://doi.org/10.1002/cite.200303260
27. Le Moullec, Y., Potier, O., Gentric, C., Leclerc, J.: Flow field and residence time distribution simulation of a cross-flow gas-liquid wastewater treatment reactor using CFD. Chem. Eng. Sci. **63**, 2436–2449 (2008)
28. Gleiss, M., Nirschl, H.: Modeling separation processes in decanter centrifuges by considering the sediment build-up. Chem. Eng. Technol. **38**, 1873–1882 (2015)
29. Stahl, S., Spelter, L.E., Nirschl, H.: Investigations on the separation efficiency of tubular bowl centrifuges. Chem. Eng. Technol. **31**, 1577–1583 (2008)